Open Access Journal
Journal of Power Technologies 94 (Nuclear Issue) (2014) 16–26
journal homepage:papers.itc.pw.edu.pl

Comparison of Simple Design of Sodium and Lead Cooled Fast Reactor Cores

Piotr Mazgaj*, Piotr Darnowski, Sebastian Gurgacz, Maciej Lipka, Karolina Dziubanii

Institute of Heat Engineering, Warsaw University of Technology
21/25 Nowowiejska Street, 00-665 Warsaw, Poland

Abstract

This report presents the results of a numerical simulation of thermal hydraulics processes in a liquid metal cooled fast reactor core, combined with simple neutron population computing for an infinite pin cell lattice. Two types of coolant were studied: liquid sodium and liquid lead, with all requirements regarding safety conditions observed. Temperature distributions along the cooling channel and distributions in the radial direction were prepared, then criticality calculations were performed for MOX fuel using MCNP Monte Carlo code.

Keywords: Lead fast reactor, Sodium fast reactor, Pin design, MCNP

1. Introduction

The aim of this paper is to assess and compare heat transfer in the fuel element and cooling channel of the fast neutron reactor in steady state conditions, cooled by liquid sodium and lead with specified assumptions and inlet conditions respectively. Both metal coolants can be used for fast reactor cores due to their high cooling capabilities. Additionally, they are convenient in terms of neutronic economy due to small cross sections for parasitic capture as well as very low moderation of neutrons. Those properties are crucial in fast reactor design. Sodium has a lower melting temperature than lead and better thermophysical properties, but is much more chemically active and has a lower boiling point, whereas lead is chemically inert but highly corrosive for steel. The report also shows the methodology used to achieve the goal, presenting assumptions, results and conclusions. The paper was developed at the Information Platform TEWI.

1.1. Fissile material resources

One of the problems of modern nuclear power plants is that they use only a small part of the fissile material contained in the nuclear fuel. Demand for electricity generated by nuclear power is forecast to increase, so there is a need to give consideration to enhancing the utilization of the fuel. One solution to the issue is to use Fast Breeder Reactors (FBR - when breeding is possible and FR - with no breeding) which open up the possibility of increasing the fissile material inventory by a factor of more than 60 [1].

The two most important fissile isotopes are uranium-235 and plutonium-239. Uranium-235 is found in nature (c.a. 0.7% of natural uranium). Plutonium-239 is created artificially when uranium-238 (c.a. 99.3% of natural uranium) absorbs a neutron and then the resulting nucleus undergoes two beta minus decays. Thermal reactors used in contemporary power plants use uranium very ineffi-

*Corresponding author
Email address: piotr.mazgaj@itc.pw.edu.pl (Piotr Mazgaj*)

ciently. According to the International Atomic Energy Agency, demand for nuclear power will increase by 25% in the low projection and by 100% in the high projection [2]. Total identified resources of uranium are sufficient for over 100 years of supply based on current requirements [3]. So the question is what should be done to increase fuel usage. One solution is to introduce fast reactors into the nuclear fleet. FBRs with their capability to breed nuclear fuel are able to provide energy for the next thousand years with already known uranium sources [4]. In the face of limited resources of uranium and increasing demand for nuclear power, there is a need for new nuclear systems.

1.2. Development of fast reactors

The first fast reactor called Clementine was constructed in 1946 in the USA. The core was cooled by mercury and was decommissioned due to a breakdown in 1952. The next fast reactor cooled by mercury was BR-2 built in 1956 in the USSR. Similarly to the Clementine, the BR-2 was damaged. Due to its strong corrosive effect, mercury is no longer used or considered for use as a coolant in reactors. Later, liquid sodium and sodium-potassium alloy (NaK) were very extensively used as coolants for FRs except for reactors used in Alfa-class submarines cooled by lead-bismuth eutectic (LBE). A list of the most important fast reactors built to date is presented in Table 1.

The idea of building a whole fleet of fast breeder reactors gained momentum in the early 1970s, when nuclear power was expected to develop significantly and there were concerns of a rapid exhaustion of the world's uranium resources. The rate of development of nuclear power reduced in the late 1980s and interest in FBRs decreased. There were many reasons for this, but the most important are: reductions in nuclear arsenals, proliferation and reprocessing policies, the Three Mile Island and Chernobyl accidents and political changes in Eastern Europe including the demise of the USSR. Moreover, and perhaps most importantly, predictions of looming fossil fuel shortages were shown to be utterly wrong.

The Generation IV International Forum (GIF) is a cooperative international endeavor, organized to carry out the research into the next generation nuclear energy systems. GIF has identified and selected six nuclear energy systems for further development. Three of the proposed generation IV reactor types are fast spectrum reactors [7]:

- Gas-Cooled Fast Reactor (GFR)
- Sodium-Cooled Fast Reactor (SFR)
- Lead-Cooled Fast Reactor (LFR)

With the establishment of GIF in 2001 and the launch of the project to design and build generation IV reactors, research on FRs has intensified. Most designs, perhaps surprisingly, are not pure breeder reactors but converter reactors, designed for efficient utilization of nuclear fuel. Additionally, some FRs are designed as burner reactors with plutonium and minor actinides transmutation capability purposed to reduce the radiotoxicity of spent nuclear fuel and close the nuclear fuel cycle [1]. Subject to consideration as coolants for the new generation of fast reactors are: helium, sodium, lead and LBE.

1.3. Coolants properties

Basic thermophysical parameters of sodium, lead and LBE such as their melting and boiling points enable the safe operation of FR at standard atmospheric pressure at primary cooling circuit temperatures of between 400°C and 600°C. One of the most important disadvantages of liquid metals is the fact that the melting temperature is so high that the cooling system must be heated to prevent solidification of the metal during shutdown. This problem does not occur in the case of, for example helium, where change of the physical state in the core is impossible.

LBE or lead coolant velocity is limited by erosion concerns of protective oxide layers to about 2.5–3.0 m/s. Typical sodium velocities are up to 8–10 m/s, hence lead has, in practice, a lower heat removal capacity [8]. Sodium, lead and LBE introduce a small amount of parasitic absorption. Fast neutrons in contact with the nuclei of these metals show a small moderation. In addition, lead and LBE are very good neutron reflectors. Hence, we can also infer that the neutron economy of the lead-alloy-cooled systems would be better than for sodium-cooled counterparts having the same geometry. For

example, lead-alloy-cooled, fuelled systems require smaller plutonium enrichments than sodium counterparts to reach criticality condition [9].

Despite the small neutron capture during irradiation, both sodium and LBE forms radioactive isotopes. The sodium (Na-23) absorbing neutron is transmuted to Na-24, which is a strong gamma emitter with a half-life of 15 hours. Bismuth-209 turns into bismuth-210, which decays to polonium-210 and it is a strong alpha emitter and could form dangerous volatile compound during accident conditions [1]. Moreover, polonium element is very toxic, but it rapidly forms a stable compound with lead - PbPo, which is well retained in the Pb-Bi coolant ([10]).

An interesting cross-comparison of fast reactor coolants for Gen-IV systems was presented by Hejzlar [11]. Recent and extensive discussion of selection of coolants is presented in the work of Sakamoto et. al [12]. A comparison of sodium and lead in respect of reactor physics, safety and economics was discussed in article [8].

2. Methodology

2.1. Basic design

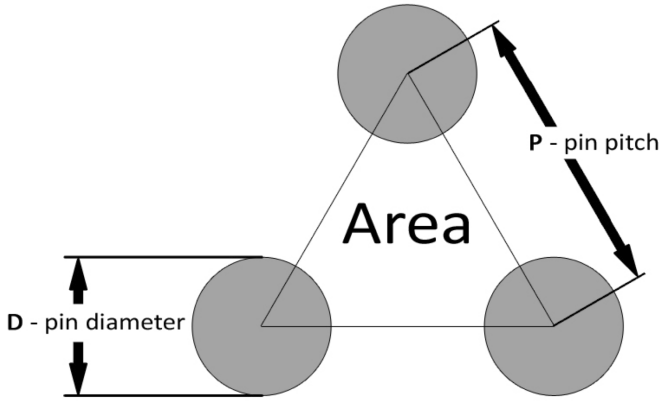

Figure 1: The geometry of single reactor cooling channel

The geometry of the fuel pin was set up early on in the analysis. Due to the selected hexagonal lattice the unit cell is triangular, as is typical for fast reactors. The following dimensions were assumed: fuel rod active length, pin diameter, cladding thickness, gas gap thickness and pin to pitch ratio. The geometrical arrangement is presented in Fig. 1 and Table 2.

The next step was to set the coolant inlet parameters: temperature and velocity. To have a reasonable margin, velocities of 8 m/s and 1.5 m/s for sodium and lead respectively were selected. Due to the difference in coolant flow velocities, the hydraulic diameter for lead had to be greater than that for sodium because the increased flow area leads to improved heat removal capabilities. Finally P/D (pitch-to-diameter, as depicted in Fig. 1) ratios corresponding to velocities were set at 1.2 and 1.6 for sodium and lead respectively.

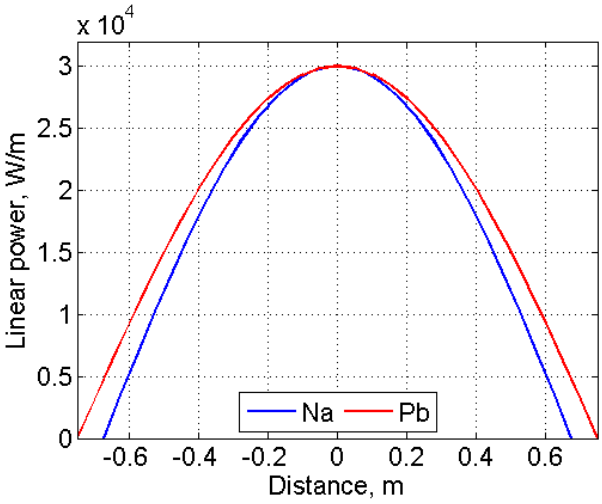

Figure 2: Power density profiles used in calculations

Table 2: Basic assumptions and design parameters

Coolant	Sodium	Lead
Rod active length, m	1.0	
Pin diameter, cm	0.61	
Cladding thickness, cm	0.4	
Gas gap thickness, cm	0.015	
Max. linear power density, W/m	300	
Inlet coolant temperature, K	673	
Coolant velocity, m/s	8.0	1.5
P/D ratio	1.2	1.6

The next parameter to be determined was the peak linear power density, and the value 30 kW/m was selected. The axial power profile was approximated by chopped cosine, as it is for neutron flux distribution in a bare core without reflector [15]. Extrapolation length was set to 35% of the radius for

Table 3: Alloying elements of ferritic-martensitic T91 steel, wt.%. [13]

Cr	Mo	Si
8.35	1.03	0.45
V	Mn	Fe
0.202	0.47	remaining part

Table 4: Alloying elements of D-9 austenitic steel, wt.% [14]

Cr	Ni	Mo
15	15	1.2
Si	Mn	Ti
0.6	1.5	0.4
C	P	Fe
0.1	0.03	remaining part

sodium and 50% for lead as a reasonable approximation [16]. Coolant inlet temperature was 673 K, which is the temperature to avoid solidification of lead with proper margin and same temperature was set for sodium. For the sodium coolant an austenitic steel D-9 [14] was selected. With respect to the corrosion produced by liquid lead, a ferritic-martenisitic steel T91 [13] was selected as a cladding material, in light of its ability to form a Cr-oxide protective layer on the cladding surface and its better performance than austenitic steel. The composition of the austenitic steel is shown in Table 3 and the ferritic-martensitic in Table 4. The assumptions and the design parameters are presented in Table 2. As was mentioned earlier, the power density distribution profiles presented in Fig. 2 are both described by a cosine functions, but in the case of lead as a coolant there is a higher flux extrapolation length because it reflects more neutrons into the core than sodium does [8, 16].

2.2. Neutronics calculations

Geometry and the material content were inputted into MCNP5 Monte Carlo code to achieve the neutron multiplication factor for a radially infinite pin cell lattice and to find an adequate geometrical configuration to complete the design process [17]. In the established model, the 1.5 m layers of coolant above and under the reactor core were added to take into account the finite size of the reactor in the axial direction. The reflection boundary condition was stated on radial boundaries of the system. In the next step, the effective multiplication factor (criticality) was estimated by simple radial leakage relations [15, 18].

Table 5: The fuel vectors of Pu and U used in calculations [19]

Plutonium		Uranium	
Isotope	Atom. fraction, %	Isotope	Atom. fraction, %
^{238}Pu	2.3477	^{234}U	0.0031
^{239}Pu	57.0151	^{235}U	0.4091
^{240}Pu	26.9515	^{236}U	0.0101
^{241}Pu	6.0693	^{238}U	99.5777
^{242}Pu	7.6164		

The composition of the MOX fuel, expressed in atomic fractions of the components, was 20% of plutonium and 80% of depleted uranium. Thus plutonium enrichment is relatively high and should provide an acceptable amount of excess reactivity. The oxygen to metal ratio (O/M) was assumed at 1.98 to provide proper substechiometry. Moreover, fuel density was 10.559 g/cm^3 and it was 95% of theoretical density for used isotope vectors. The fuel was composed of recycled plutonium and depleted uranium, the uranium being made from spent PWR fuel with initial enrichment of 4.5% and burned to 45 MWd/kg after 15 years of cooling [19]. Uranium and plutonium fuel vectors are presented in Table 5. Critically calculations were accomplished only for the beginning of life (BOL) fuel state, which means that fuel was taken as fresh.

Effective multiplication factor keff was roughly estimated for a core with radius of 1 m using Eq. 1 as for a bare cylindrical core without reflector by estimation of P_{NL}—probability of non-leakage [15, 20]:

$$k_{eff} = P_{NL} k_\infty = \frac{k_\infty}{1 + L^2 B^2} \tag{1}$$

where k_∞ is multiplication factor obtained with MCNP5 for a radially infinite system (not infinite in the axial direction), $B = (\frac{2.4048}{R})^2$—geometric buckling for an infinite length cylinder with $R = R_0 + a$,

where a is extrapolation length in the radial direction and it was assumed to be 25 cm, R_0 is cylinder radius, L—diffusion length for neutrons.

Diffusion length was assumed at 15 cm and 18 cm for sodium and lead respectively. The analyzed system is infinite in the radial direction but not in the axial direction, so PNL is calculated as for an infinite length cylinder to estimate leakage in the radial direction [15].

2.3. Thermalhydraulic model

The isolated subchannel approach was applied to perform calculations in this paper. It is a rather simple methodology used in general only for preliminary calculations. For the purposes of more reasonable computations and modern TH design process of the fuel element, entire assembly analysis with subchannel codes and/or additional three dimensional Computational Fluid Dynamics (CFD) analysis should be performed [21]. The subchannel approach is presented in a fast reactor reference book by Waltar [1] and a recent example of fuel assembly subchannel analysis can be found in [22] and CFD computations [23].

The temperature dependence of thermal conductivity used in this work was for the MOX fuel with 20% Pu enrichment and 95% theoretical density with an oxide-to-metal ratio of 2.0 described in [1]. A review of detailed MOX fuel thermophysical properties can be found in [24].

Maximum fuel temperature of 2520 K for oxide fuel was used as suggested by Sobolev [25]. It gives a reasonable margin to liquidus temperature, equal to 3063 K for MOX with 20% Pu [1].

The thermal conductivity of cladding steels D-9 and T91 were taken from [26] and [13] respectively. Cladding conductivity was set as constant due to the small thickness of cladding and small temperature gradient in it. Cladding conductivity temperature dependencies are rather weak and for simplicity, values for 700 K were assumed: 19.9745 $\frac{W}{mK}$ for D-9 and 28.87 $\frac{W}{mK}$ for T91. More issues in cladding selection for FR are discussed in Cheon et al. [27].

In the situation when the gas gap between fuel and cladding is still open (in relatively fresh fuel), three fundamental modes of heat transfer can appear: radiation, conduction and convection. Nevertheless, temperature is still relatively low and during normal operation the heat conduction mechanism is superior. The same occurs when the gas gap is closed [1]. In this communication, the heat transfer coefficient is 6000 $\frac{W}{m^2K}$, which is a rather conservative value suggested by Sobolev [25]. It is necessary to remember that the gas gap heat transfer changes due to fuel irradiation and temperature effects (restructuring). The composition of gas in the gap is also significant, because it changes with the irradiation level. Gaseous fission products have lower thermal conductivity and they cause the gas gap thermal conductivity to decrease. When the fuel swells, the gas gap slowly disappears and subsequently the heat transfer between the fuel and cladding changes. The direction of change is the result of positive (swelling of the fuel) and negative (increasing concentration of gaseous fission products) effects. A detailed description of the processes involved can be found in [1].

The typical coolant temperatures in SFR are for core inlet in the region of 640 K and for core outlet 820 K [28]. Note that the melting point of sodium at atmospheric pressure is 370 K, while the melting point of lead is much higher (600.6 K). In the case of liquid lead there are some additional constraints. The recommended minimum coolant temperature is about 673 K [25] and its solidifying temperature at atmospheric pressure is 600.6 K, so the margin is relatively lower in this case. Maximum lead temperature is governed by corrosion issues; for ferritic-martensitic steel corrosion occurs at the temperature of 823 K [25]. Working temperatures for both reactors are very similar and it was assumed that the core inlet temperatures for both SFR and LFR are the same, at 673 K.

The liquid sodium and the liquid lead densities used in this model were taken from Waltar et al. [1] and Wallenius [16] respectively. Heat transfer coefficients were obtained by Nusselt number correlation for liquid metal flow through tube bundles (both Na and Pb) and described in a recent review article by Mikityuk [29]. Discussion of the various liquid metals heat transfer correlations can be found in Pfrang and Struwe's work [30]. Specific heat capacities for correlations of both coolants were taken from [16].

The thermal-hydraulics model created was one dimensional, single phase and for steady state condi-

tions. The mathematical formulation for this model was based on the one described in [15, 31–33]. The first goal was to compute temperature distribution along the cooling channel to assess its performance. The second goal was to compute temperature distribution in the radial direction - fuel, gap and cladding for the given coolant bulk temperature. In order to obtain the axial temperature profile for the coolant, the channel was divided into 20 control volumes of equal length. All necessary equations were coded in the MATLAB environment and iteration produced the results.

The mass conservation equation is given by the equation:

$$\frac{d(GA)}{dx} = 0 \tag{2}$$

due to assumption of constant flow area A, it leads to constant mass flux G. Equation 2 gives the possibility to calculate flow velocity (u) based on the relation: $G = \rho u$, where $\rho = \rho(T)$ is liquid metal density which is a function of temperature and changes from node to node. The momentum equation was not solved in this model because the pressure drops were not analyzed. The simple energy equation was considered in the following form:

$$GA\frac{dh(x)}{dx} = q'(x) \tag{3}$$

where h is coolant enthalpy and q' is linear heat flux, which is in the form of the chopped cosine:

$$q'(x) = q'_0 cos(\frac{\pi x}{H_e}) \tag{4}$$

where H_e is extrapolation length and q'_0 is peak linear heat flux. The energy equation was solved for every node by integration of Eq. 4. Enthalpy change between nodes: $(h_{i+1} - h_i)GA$ was equal to power (q_i) transferred from the nuclear fuel to the coolant:

$$(h_{i+1} - h_i)GA = q_i = \int_{x_i}^{x_{i+1}} q'(x)dx \tag{5}$$

In order to obtain a temperature increase according to the known enthalpy increase in single control volume, the following integral can be solved iteratively for T:

$$h_{i+1} - h_i = \int_{T_i}^{T_{i+1}} c_p(T)dT \tag{6}$$

Those methods make it possible to obtain temperature distribution along the reactor cooling channel. It is worthwhile mentioning that there are simpler and more efficient approaches to find those distributions [16]. Integration performed separately on every node interval is computationally inefficient.

In order to achieve the second goal, it was necessary to assume that there is no axial heat transfer in the fuel element—and it is quite a reasonable approximation for a nuclear reactor working in normal conditions. For every axial control volume, inner iterations for radial temperature distribution were performed and coolant bulk temperature (Eq. 7) was used in order to couple thermally cladding with coolant by using Newton's law of cooling:

$$q'' = \frac{q'}{\pi D_{clad}^{outer}} = h_{cool}(T_{clad}^{outer} - T_{bulk}) \tag{7}$$

where D_{clad}^{outer} is cladding diameter and q'' is heat flux on the cladding surface. The Nusselt number provides heat transfer coefficient: $h_{cool} = Nu\frac{\lambda_{clad}}{D_h}$ [31, 32]. The Nusselt number is a function of the Peclet number only, which is specific for liquid metals [29]:

$$Nu = 0.047(1 - e^{-3.8(\frac{P}{D}-1)})(Pe^{0.77} + 250) \tag{8}$$

where P/D is pitch-to-diameter ratio and the Peclet number is given by relation: $Pe = \frac{Gc_pD_h}{\lambda}$ and D_h is the hydraulic diameter. The inner cladding temperature was computed by the typical solution of the heat conduction equation in cylindrical wall with constant thermal conductivity:

$$T_{clad}^{inner} = T_{clad}^{outer} + \frac{q'}{2\pi\lambda_{clad}} ln(D_{clad}^{outer}/D_{clad}^{inner}) \tag{9}$$

Substituting D_{clad}^{outer} with variable D gives a possibility to find temperature profile in the cladding.

The exact temperature profile in the gas gap is not obtainable without taking into account the whole heat transfer mechanism. To find the fuel pellet outer temperature Newton's law of cooling should be used:

$$T_{pellet}^{outer} = T_{clad}^{inner} + \frac{q'}{\pi D_{pellet} h_{gap}} \tag{10}$$

The last step was to find the fuel pellet temperature profile and fuel centerline temperature. In the case of constant fuel thermal conductivity the temperature profile has a simple parabolic shape. Nevertheless, for oxide fuel there are enormous temperature gradients in the pellet and a more complicated approach should be involved. The fuel centerline temperature (T_{CL}) can be obtained by iterative solution of the conductivity integral [1, 15, 31, 32]:

$$q' = 4\pi \int_{T_{pellet}^{outer}}^{T_{CL}} \lambda_{fuel}(T) dT \tag{11}$$

The fuel pellet temperature profile can be calculated if the pellet is radially divided into the set of nodes (in those simulations it was 10) and the fact used that: $q' = \pi r^2 q'''$ with an assumption of constant power density (q'''). The important issue is that density is not constant inside the fuel pellet due to intense absorption in the outer fuel region, which impacts reactor power. The following integral is solved iteratively in order to find temperature distribution:

$$\frac{1}{4\pi} q' \left(\frac{r}{D_{pellet}/2}\right)^2 = \int_{T(r)}^{T_{CL}} \lambda_{fuel}(T) dT \tag{12}$$

where r is radius inside the fuel pellet both with corresponding temperature $T(r)$.

Table 6: Results obtained from the numerical calculations

Coolant	Sodium	Lead
Coolant outlet temperature, K	730	765
Max. outer cladding temperature, K	739	803
Max. inner cladding temperature, K	758	817
Max. fuel outer surface temperature, K	982	1036
Max. fuel temperature in the pellet center, K	1896	1970
Criticality for the infinite pin lattice	1.31729	1.22576
Criticality standard deviation	0.00050	0.00044
Effective criticality (estimation)	1.21602	1.09451

3. Results

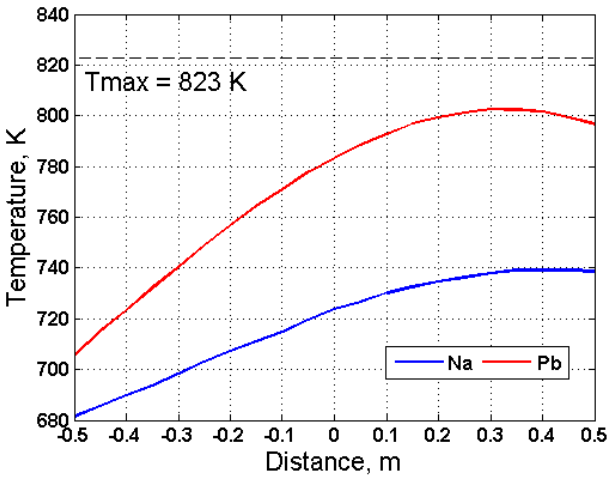

Figure 3: Cladding outer temperature profile

The results of the calculations, briefly described in the methodology, were summarized in Table 6 and in a set of charts showing certain parameters of axial profiles for heat transfer in liquid sodium and lead (Fig. 3–10).

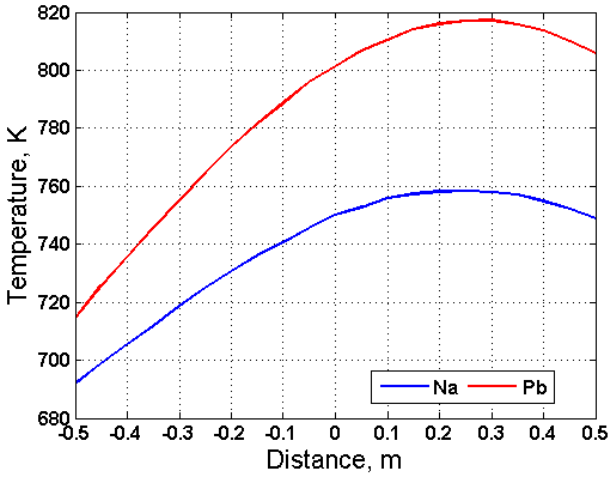

Figure 4: Cladding inner temperature profile

The cladding external temperature profile is presented in the Fig. 3 and the cladding internal temperature on Fig. 4. As it can be seen, the outlet temperature for lead coolant is noticeably higher than for sodium coolant (1036 K and 982 K respectively). At this point it can be clearly proven, that the heat removal ability of sodium is higher due to its higher heat transfer abilities.

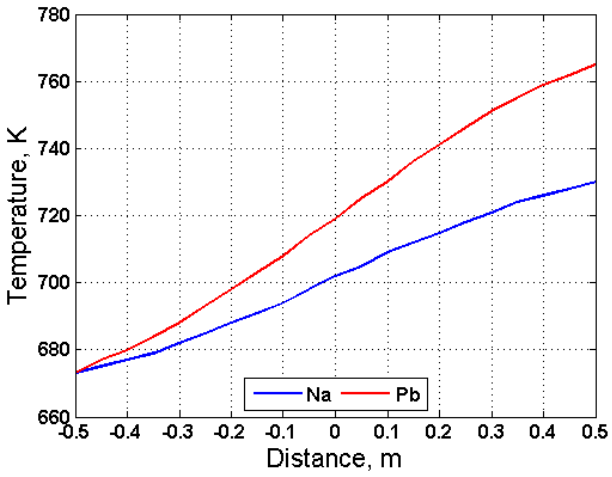

Figure 5: Axial coolant temperature distribution through the channel

Distribution of temperature in coolants as presented in Fig. 5 supports this statement, and as can be seen, the temperature of lead at the outlet is noticeably higher than the temperature of sodium (765 K and 730 K respectively), which is due to sodium's better heat transfer characteristics.

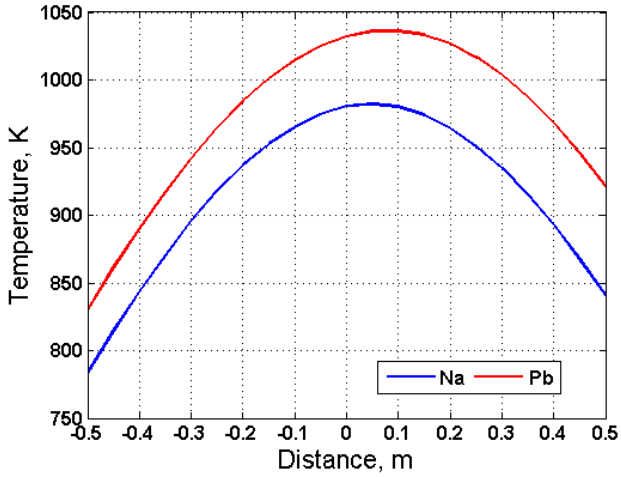

Figure 6: Fuel outer surface axial temperature profile

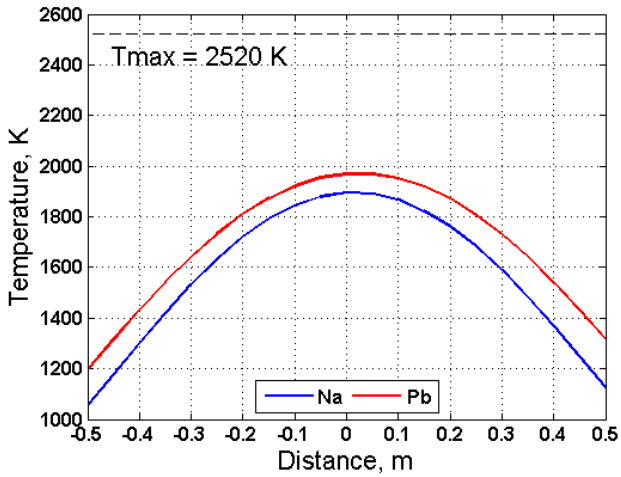

Figure 7: Fuel centerline axial temperature profile

In Fig. 7 the fuel temperature distribution in the fuel pellet is presented. As it can be seen, the fuel temperature for lead coolant is about 80 K higher and reaches a maximum axial value of 1970 K, versus only 1896 K for the sodium coolant respectively. The profile is slightly asymmetrical and has higher values for the half part that is closer to the coolant outlet. The fuel outer surface presents (Fig. 6) the same trend, as is expected for oxide fuel, the radial temperature gradient is high. For sodium in the maximum centerline temperature the gradient is 914 K, and for lead it is 934 K so those values are comparable.

Fig. 8 shows the radial temperature distribution in the fuel pin. It is possible to observe a high margin

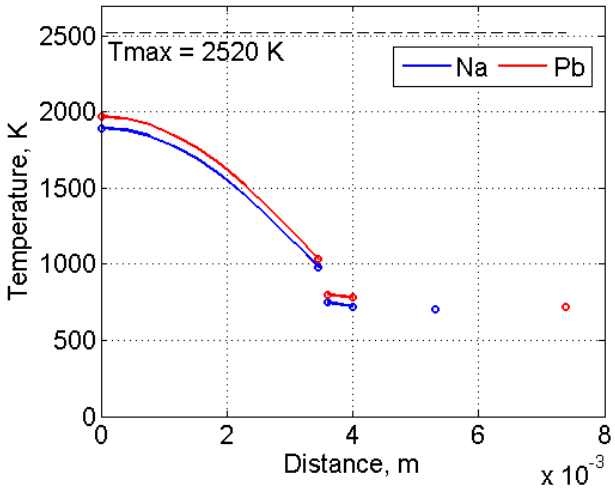

Figure 8: Fuel radial temperature profile in the hottest section of the fuel pin. Outermost circles correspond to coolant bulk temperatures

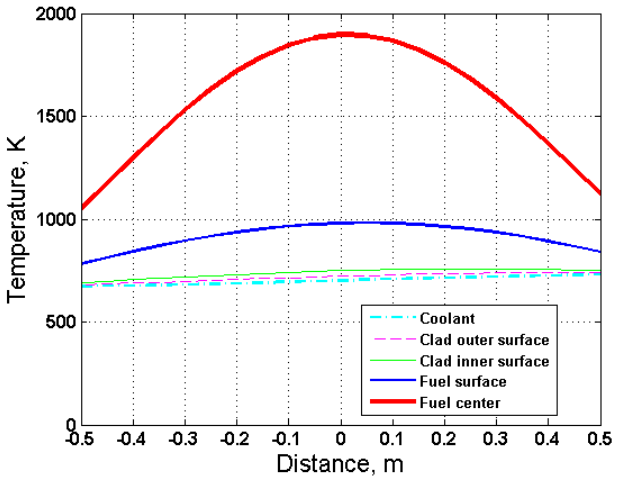

Figure 9: Comparison of sodium temperature profiles

to the assumed maximum fuel temperature and it can be concluded that for those channel configurations it is possible to utilize much higher linear power. Expected semi-parabolic profiles in the fuel and logarithmic cladding temperature were obtained (Fig. 8).

The fuel and the cladding radial temperature profiles were calculated. For the gas gap and the coolant, only the boundary temperatures were calculated, due to Newton's approach, which does not allow one to calculate the temperature profile. Statements of all temperature profiles in axial direction are presented for sodium and lead on Fig. 9 and Fig. 10 respectively.

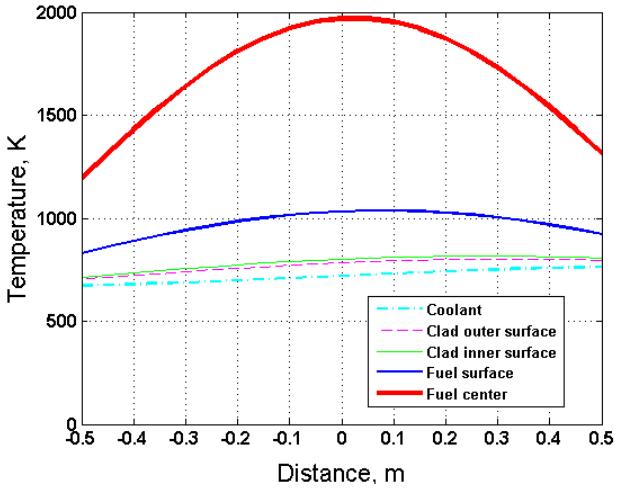

Figure 10: Comparison of lead temperature profiles

4. Conclusions

The results obtained seem compatible with the data presented in the available literature. Although sodium has some disadvantages, such as high chemical reactivity and worse neutron reflection properties than lead, the thermal hydraulics analysis has confirmed that with respect to thermo-physical properties, liquid sodium coolant is superior to lead. The main advantages are: better heat removal capabilities as well as both lower fuel and cladding temperatures. These features together with the higher flow velocity of sodium lead to higher linear power being available and a lower pitch to diameter ratio required. Moreover, in terms of use as coolants, far greater technological and operational experience has been amassed for sodium than for lead over the past half century.

[1] D. T. P. T. A.E. Waltar, A. Reynolds, Fast Spectrum Reactors, Springer, 2011.
[2] IAEA, International status and prospects for nuclear power 2012, Tech. rep., IAEA (2012).
[3] IAEA, Uranium 2011: Resources, Production and Demand, A Joint Report by the OECD Nuclear Energy Agency and the International Atomic Energy Agency, 2012.
[4] SNETP, Esnii concept paper, Tech. rep., Sustainable Nuclear Energy Technology Platform, http://www.snetp.eu (2010).
[5] World nuclear association reactor database. URL `http://world-nuclear.org`
[6] Iaea power reactor information system. URL `http://www.iaea.org/pris`
[7] G. I. I. Forum, A technology roadmap for generation iv nuclear energy systems, http://www.gen-4.org (2002).

[8] K. Tucek, J. Carlsson, H. Wider, Comparison of sodium and lead-cooled fasr reactors reagarding physics aspects, svere safety and economical issues, Nuclear Engineering and Design (236) (2006) 1589–1598.

[9] K. Tucek, Neutronic and burnup studies of accelerator-driven systems dedicated to nuclear waste transmutation, Ph.D. thesis, Royal Institute of Technology, Stockholm (2004).

[10] V. Sobolev, Myrrha ads database: Part i. thermophysical properties of molten lead-bismuth eutectic, Tech. rep., SCK, CEN (2005).

[11] P. Hejzlar, N. Todreas, E. Schwageraus, A. Nikiforova, R. Petroski, M. Driscoll, Cross-comparison of fast reactor concepts with various coolants, Nuclear Engineering and Design (239) (2009) 2672–2691.

[12] Y. Sakamoto, J. C. Garnier, J. Rouault, C. Grandy, T. Fanning, R. Hill, Y. Chikazawa, S. Kotake, Selection of sodium coolant for fast reactors in the us, france and japan, Nuclear Engineering and Design 254 (2013) 194–217.

[13] R. Williams, R. Graves, D. McElroy, Thermal and electrical conductivities of an improved 9 Cr-1 Mo steel from 360 to 1000 K, International Journal of Thermophysics 5 (3) (1984) 301–313.

[14] J. S. Cheon, C. Lee, B. O. Lee, J. Raison, T. Mizuno, F. Delage, J. Carmack, Sodium fast reactor evaluation: Core materials, Journal of Nuclear Materials (392) (2009) 324–330.

[15] M. Kiełkiewicz, Teoria Reaktorów Jądrowych, Oficyna Wydawnicza Politechniki Warszawskiej, 1987.

[16] J. Wallenius, Transmutation of nuclear waste, Roayal University of Technology, Stockholm, http://neutron.kth.se/courses/transmutation/TextBook.shtml, 2010.

[17] T. Goorley, Criticality calculations with MCNP5: A primer, Tech. Rep. LA-UR-04-0294, Los Alamos National Laboratories X-5 (2004).

[18] A. Waltar, A. Reynolds, Fast Breeder Reactors, Pergamon Press, 1981.

[19] P. Mazgaj, Conceptual neutronic design of a 300 MWth lead fast reactor core, Master's thesis, Warsaw University of Technology (2010).

[20] E. Lewis, Fundamentals of Nuclear Reactor Physics, Academic Press, 2008.

[21] H. Anglart, Applied Reactor Technology, Institute of Heat Engineering, 2013.

[22] Y. W. Wu, X. Li, X. Yu, S. Z. Qiu, F. Su, W. Tian, Subchannel thermal-hydraulic analysis of the fuel assembly for liquid sodium cooled fast reactor, Progress in Nuclear Energy 69 (2013) 65–78.

[23] K. D. Hamman, R. A. Berry, A cfd simulation process for fast reactor fuel assemlies, Nuclear Engineering and Design 240 (2010) 2304–2312.

[24] J. Carbajo, G. Yoder, S. Popov, V. Ivanov, A review of the thermophysical properties of MOX and UO_2 fuels, Nucl. Mater. 299 (299) (2001) 181–198.

[25] V. Sobolev, E. Malambu, H. A. Abderrahim, Design of a fuel element for a lead-cooled fast reactor, Journal of Nuclear Materials (385) (2009) 392–399.

[26] L. Leibowitz, R. A. Blomquist, Thermal conductivity and thermal expansion of stainless steels d9 and ht9, International Journal of Thermophysics 9 (5) (1988) 873.

[27] J. S. Cheon, C. Lee, B. O. Lee, J. P. Raison, T. Mizuno, F. Delage, J. Carmack, Sodium fast reactor evaluation: Core materials, Journal of Nuclear Materials 392 (2009) 324–330.

[28] IAEA, Iaea fast reactor database (2012).

[29] K. Mikityuk, Heat transfer to liquid metal: Review of data and correlations for tube bundles, Nuclear Engineering and Design 239 (2009) 680–687.

[30] W. Pfrang, D. Struwe, Assessment of Correlations for Heat Transfer to the Coolant for Heavy Liquid Metal Cooled Core Designs, Forschungszentrum Karlsruhe Gmbh, 2007.

[31] N. Todreas, M. S. Kazimi, Nuclear Systems: Vol. I, Thermal Hydraulic Fundamentals, Taylor & Francis, 1990.

[32] H. Anglart, Thermal-Hydraulics in Nuclear Systems, Institute of Heat Engineering, 2013.

[33] S. Levy, Two-Phase Flow in Complex Systems, John Wiley &Sons, 1999.

Table 1: List of the most important fast reactors built to date (source: [5, 6])

Facility	Country	Ther.power, MW	El.output, MWe	Operation	Coolant
Clementine	USA	0.025	-	1946–1952	mercury
BR-2	USSR	0.1	-	1956–1958	mercury
BM-40A*	USSR	155	-	1969–1990	LBE
BN-350	Kazakhstan	1000	90	1972–1999	sodium
Phenix	France	345	142	1973–2010	sodium
BN-600	Russia	1470	600	1980–pres.	sodium
Superphenix	France	3000	1242	1985–1998	sodium
Monju	Japan	714	280	1994–1995	sodium

*used in Alfa-class submarines